

# Generation Models Know Space: Unleashing Implicit 3D Priors for Scene Understanding

Xianjin Wu<sup>1</sup>, Dingkang Liang<sup>1†</sup>, Tianrui Feng<sup>1</sup>, Kui Xia<sup>2</sup>, Yumeng Zhang<sup>2</sup>, Xiaofan Li<sup>2</sup>, Xiao Tan<sup>2</sup>, and Xiang Bai<sup>1</sup>

<sup>1</sup> Huazhong University of Science and Technology

<sup>2</sup> Baidu Inc., China † Project Lead

{wuxianjin,dkliang}@hust.edu.cn

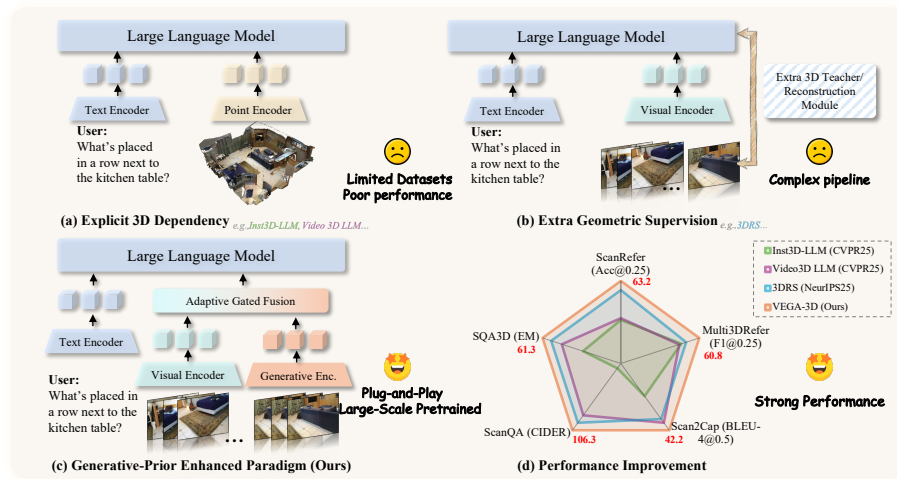


**Fig. 1: Comparison of existing paradigms.** Unlike methods relying on (a) explicit 3D inputs or (b) complex geometric supervision, (c) our **VEGA-3D** extracts implicit priors from video generation models. By repurposing them as Latent World Simulators, we achieve (d) superior performance without external 3D dependencies.

**Abstract.** While Multimodal Large Language Models demonstrate impressive semantic capabilities, they often suffer from **spatial blindness**, struggling with fine-grained geometric reasoning and physical dynamics. Existing solutions typically rely on explicit 3D modalities or complex geometric scaffolding, which are limited by data scarcity and generalization challenges. In this work, we propose a paradigm shift by leveraging the implicit spatial prior within large-scale video generation models. We posit that to synthesize temporally coherent videos, these models inherently learn robust 3D structural priors and physical laws. We introduce **VEGA-3D** (Video **EX**tracted **GE**nerative **A**wareness), a plug-and-play framework that repurposes a pre-trained video diffusion model as a Latent World Simulator. By extracting spatiotemporal features from intermediate noise levels and integrating them with semantic representations via a token-level adaptive gated fusion mechanism, we enrich MLLMs with dense geometric cues without explicit 3D supervision. Extensive experiments across 3D scene understanding, spatial reasoning, and em-

bodied manipulation benchmarks demonstrate that our method outperforms state-of-the-art baselines, validating that generative priors provide a scalable foundation for physical-world understanding. Code is publicly available at <https://github.com/H-EmbodVis/VEGA-3D>.

**Keywords:** Video Generation Models · 3D Scene Understanding · Spatial Reasoning · Embodied AI

## 1 Introduction

Recent advancements in video generation models [3, 33, 37, 44, 66] have reshaped our expectations of visual systems, moving beyond high-fidelity generation to acting as interactive world models [38, 65, 70]. To generate a plausible video, the model inherently aligns appearance with 3D geometry: occlusion requires persistent object identity, camera motion reveals depth-dependent apparent motion, and interactions must follow consistent dynamics. These constraints encourage latent representations that encode geometry-consistent structure and motion, yielding a strong learned 3D prior without explicit 3D supervision [39, 60]. This raises a compelling research question: if video generators already possess an implicit understanding of space and physics, can these implicit physical priors be repurposed to improve downstream 3D visual understanding?

This perspective is particularly critical for domains that require granular 3D awareness [7, 25, 51, 72, 88], such as scene understanding. To equip embodied agents with such capabilities, prevailing research has predominantly followed two explicit paradigms, as illustrated in Fig. 1. The first stream [77, 87] directly utilizes explicit 3D modalities, incorporating point clouds or depth to provide definitive geometric grounding [27, 56, 71, 92]. The second stream [16, 34, 67] focuses on geometric scaffolding, which lifts 2D features into 3D space via extra reconstruction or distillation. Alongside these methods, an underexplored yet increasingly promising paradigm (Fig. 1(c)) lies in modern video generation models trained on large-scale video datasets, whose training objective implicitly rewards representations consistent with 3D geometry and physical dynamics.

In this work, we explore a new paradigm: leveraging representations learned by video generation models as priors for geometric understanding. As illustrated in the Fig. 2 (a), video diffusion models demonstrate remarkable multi-view consistency. The model captures the structural integrity of objects across different frames, implying a robust internal representation of 3D geometry. While generative models lack the semantic alignment of contrastive pre-training [64, 78], their geometric priors offer unique spatial guidance. As further evidenced in Fig. 2(b), incorporating these priors sharpens the original scattered attention of the baseline, effectively serving as spatial anchors that enable precise localization for fine-grained 3D reasoning.

Motivated by these observations, we propose **VEGA-3D**, a plug-and-play framework that incorporates the strengths of semantic and generative representations. Specifically, we introduce a video generation model (e.g., Wan2.1 [66],

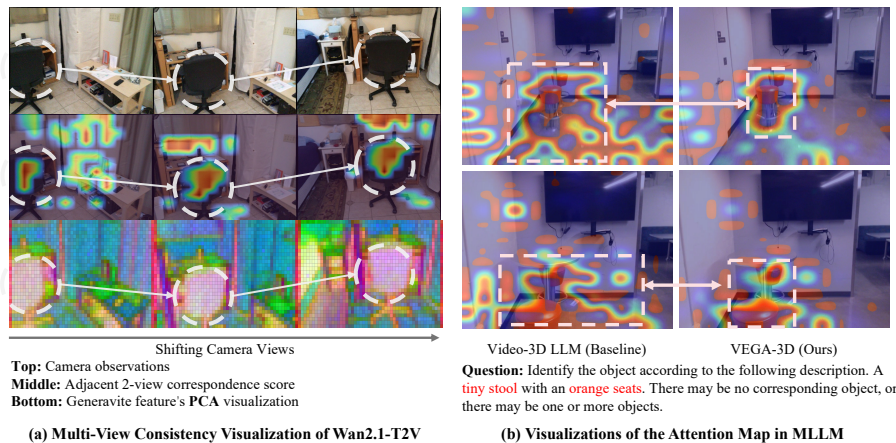


**Fig. 2: Visualization of implicit 3D priors.** (a) The generation model demonstrates strong multi-view geometric consistency, evidenced by high correspondence scores and stable PCA feature representations across shifting camera views. (b) By leveraging these priors, our **VEGA-3D** overcomes the spatial ambiguity observed in the baseline, yielding precisely-located attention maps of the target object in the instruction.

Vmem [44]) as a *Latent World Simulator* to enrich the visual stream with spatiotemporal world-knowledge priors, complementary to the semantic encoder. To solve the distribution shift between generative and semantic space, we design a token-level adaptive gated fusion module that integrates the two features. This fusion enables the model to actively exploit the generative backbone’s 3D awareness to strengthen geometry-sensitive reasoning, while preserving discriminative semantic cues.

Extensive experiments on 3D scene understanding (e.g., visual grounding, dense captioning, and QA), spatial reasoning benchmarks (e.g., VSI-Bench [73]), and robotics manipulation tasks (LIBERO [48]) demonstrate that our method significantly outperforms larger spatially-enhanced models. Furthermore, in Fig. 3, we provide quantitative evidence for the strong correlation between multi-view correspondence and downstream understanding performance. Besides, as evidenced in Fig. 3(a), the gains stem from synergy rather than replacement: generative and semantic features are complementary, and their fusion yields substantial improvements. Our analysis further shows that the most informative spatial cues emerge from intermediate representations and mid-denoising time of the generative model, instead of the final pixel outputs, and that these priors are particularly beneficial for localization-centric tasks, effectively providing a spatial anchor for MLLMs.

In summary, our contributions are threefold.

- We investigate that modern video generators learn transferable spatiotemporal priors that encode geometry-consistent structure and motion, and we show that these priors are most informative in intermediate representations and mid-denoising stages.

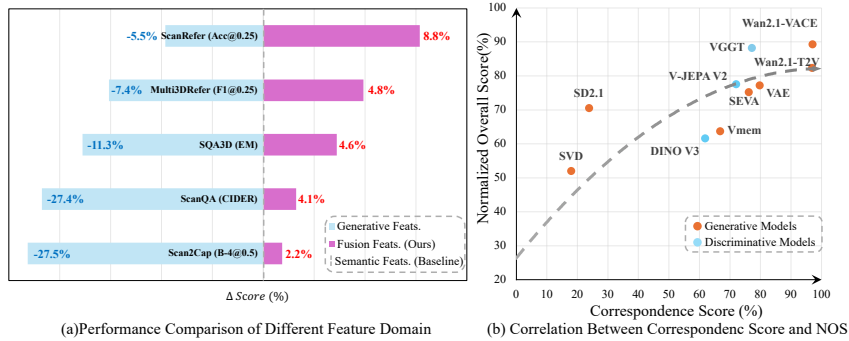


**Fig. 3: Feature Analysis.** (a): Generative priors effectively complement semantic features with fusion, yielding consistent performance gains. (b): Multi-view correspondence strongly correlates with downstream 3D understanding performance. More details in Sec. 4.1

- We propose **VEGA-3D**, a plug-and-play framework that repurposes video generation models as *Latent World Simulator* for MLLMs, and introduce a token-level adaptive gated fusion module to align and integrate heterogeneous generative and semantic token spaces.
- Extensive experiments across 3D scene understanding, spatial reasoning, and embodied manipulation benchmarks demonstrate consistent gains, validating generative priors. Moreover, our framework is scalable: advances in video generation are readily transferable to stronger downstream 3D understanding.

## 2 Related Work

### 2.1 Scene Understanding with Large Language Models

Extending Large Language Models to 3D domains is a rapidly growing field. Early approaches aligned point cloud encoders directly with LLMs [27, 30, 56, 71], as seen in PointLLM [71], Point-Bind [27], and GPT4Point [56]. While effective, they heavily depend on the availability of high-quality 3D data. To bypass the need for direct 3D input, multi-view approaches [34, 57, 67, 87, 89] like Video-3D LLM [87] and GPT4Scene [57] project 2D features into 3D space using positional embeddings or BEV rendering. More recent works attempt to lift 2D representations via auxiliary geometric supervision: Ross3D [67] utilizes reconstructive instruction tuning, while 3DRS [34] and ThinkWith3D [16] distill knowledge from pre-trained 3D backbones. However, these methods typically require complex multi-stage training pipelines or task-specific geometric annotations (e.g., depth, camera pose). In contrast, our approach leverages the implicit physical priors already present in pre-trained video generation models, eliminating the need for explicit geometric supervision or complex rendering pipelines.

## 2.2 Spatial Reasoning

While MLLMs excel at semantic recognition, they often suffer from "spatial blindness" when tasked with geometric reasoning or determining spatial relationships, as highlighted by benchmarks [36, 46, 73, 74, 81] like Sphere [81] and VSI-Bench [73]. To mitigate this, one line of research focuses on scaling data: SpatialVLM [8] and VLM-3R [22] train on massive datasets of spatial reasoning instructions to embed geometric concepts. Another direction explores mental simulation or chain-of-thought prompting, where models like MindCube [76] and CVP [15] verify spatial logic through auxiliary cognitive maps or reconstruction.

Distinct from these approaches, which treat spatial reasoning as a linguistic or logical problem, we treat it as a representational problem. By fusing generative video priors, we ground the MLLM’s reasoning in a physically consistent world model, enabling intuitive spatial understanding akin to human perception.

## 2.3 Video Generation Models

Video generation has rapidly progressed from short, low-resolution clips to high-fidelity and long-horizon synthesis powered by diffusion and transformer-based generators [5, 28, 42, 66, 75]. Recent large-scale video models [5, 42, 66] (e.g., Sora [5], Wan [66], and VideoPoet [42]) demonstrate strong temporal coherence and interaction-consistent motion, suggesting that their latent spaces capture rich spatiotemporal regularities. Beyond improving visual fidelity, a growing body of work studies how to structure and control video generators [3, 44, 60, 90]: Genie3 [3] explores latent action inference for controllable generation, while Vmem [44] introduces memory mechanisms for long-range consistency.

Different from prior efforts that mainly exploit these models for generation or control, we repurpose their implicit geometric representations as a complementary feature stream and integrate them with semantic encoders to improve discriminative 3D understanding.

## 3 Preliminaries

**Multimodal Large Language Models.** Following standard protocols [50, 59], we consider a multimodal large language model with parameters  $\Theta$ . Given a multimodal input consisting of text tokens  $\mathbf{x}$  and visual inputs  $\mathbf{V}$ , the visual content is mapped to a sequence of visual embeddings  $\mathbf{v} = f_{\text{proj}}(f_{\text{enc}}(\mathbf{V}))$ , where  $f_{\text{enc}}$  is a visual encoder (e.g., SigLIP [78]) and  $f_{\text{proj}}$  is a projector.

The MLLM is trained to maximize the likelihood of the response token sequence  $\mathbf{y}$  given the context:

$$\mathcal{L}_{\text{CE}}(\Theta) = - \sum_{i=1}^L \log p_{\Theta}(y_i | y_{<i}, \mathbf{x}, \mathbf{v}), \quad (1)$$

where  $\Theta$  denotes all trainable parameters (e.g.,  $\Theta = (\theta_{\text{lm}}, \theta_{\text{enc}}, \theta_{\text{proj}})$ ).

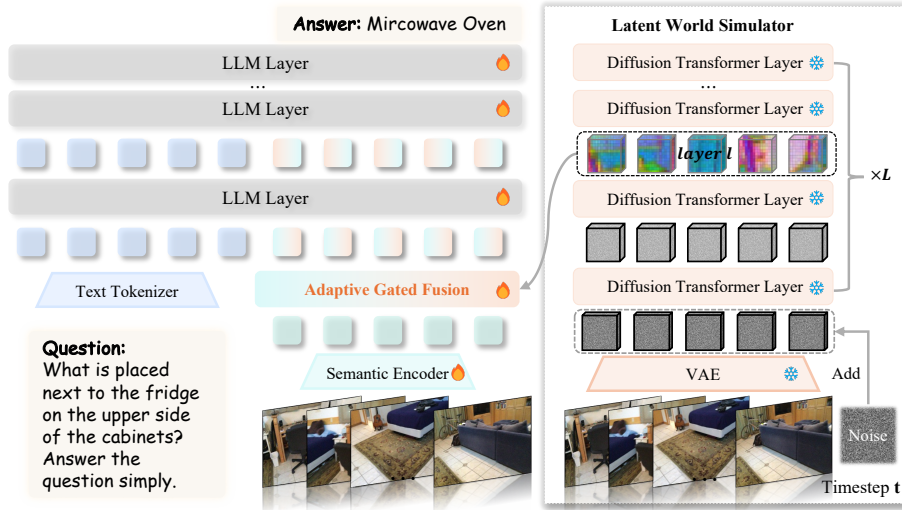


**Fig. 4: Overview of the VEGA-3D framework.** We repurpose a frozen video generation model as a **Latent World Simulator** to extract implicit 3D priors. These features are dynamically integrated with the semantic stream via **Adaptive Gated Fusion**, equipping the MLLM with dense 3D structural awareness.

Crucially, this supervision is *sparse* and *discrete* [1, 10]. The loss is computed in the vocabulary space, where spatial errors (e.g., predicting “left” vs. “right”) are treated as generic token mismatches. Lacking geometric metric constraints, standard discriminative encoders  $f_{\text{enc}}$  often exhibit “spatial blindness,” focusing on semantic presence rather than a precise spatial structure.

**Video Diffusion Models.** Modern video generators (e.g., Wan2.1 [66]) are Diffusion Transformers trained with Flow Matching [47], which learns a continuous-time transport field in the latent space. Given a clean latent video  $\mathbf{z}_0$ , we sample Gaussian noise  $\epsilon \sim \mathcal{N}(\mathbf{0}, \mathbf{I})$  and a time  $t \sim \mathcal{U}(0, 1)$ , and train a flow network  $v_\psi(\cdot)$  to regress the target velocity under MSE:

$$\mathcal{L}_{\text{FM}}(\psi) = \mathbb{E}_{\mathbf{z}_0, \epsilon, t} \left[ \|\mathbf{u}_t - v_\psi(\mathbf{z}_t, t, \mathbf{c})\|_2^2 \right], \quad (2)$$

where  $\mathbf{c}$  denotes conditioning signals. The corresponding target velocity is  $\mathbf{u}_t = \frac{d\mathbf{z}_t}{dt}$ . In implementation, we use a discrete timestep index  $k \in \{0, \dots, K\}$  (with  $K=1000$ ) and its normalized time  $t_k = \frac{k}{K}$ .

## 4 Method

Our goal is to endow Multimodal Large Language Models (MLLMs) with the implicit generative prior inherent in video generation models. As illustrated in Fig. 4, our framework introduces a dual-branch visual encoding mechanism that

synergizes the high-level semantic capabilities of a discriminative encoder (e.g., SigLIP [78]) and dense 3D structure priors from a generative video diffusion model (e.g., Wan2.1 [66]). The methodology is organized into three logical stages: (1) **3D Awareness Analysis** (Sec. 4.1), where we identify multi-view feature consistency as the key indicator of geometric capability; (2) **Latent World Simulation** (Sec. 4.2), which operationalizes these insights by mining spatiotemporal geometry from the generator’s intermediate representations via noise injection; and (3) **Bridging the Generative and Semantic Gap** (Sec. 4.3), which adaptively integrates these heterogeneous features via a token-level adaptive gated fusion mechanism to align with the MLLM.

#### 4.1 3D Awareness via Multi-view Feature Consistency

A pivotal factor in robust 3D scene understanding is the ability to maintain consistent representations of physical geometry across varying viewpoints. While traditional discriminative models excel at semantic invariance, we hypothesize that effective 3D reasoning often benefits from multi-view feature consistency, which maps the same physical 3D point to a unified latent representation across different views. To quantitatively verify this correlation and evaluate the geometric integrity of different feature backbones, we introduce **Multi-view Correspondence Score**.

**Metric Definition.** We utilize the ScanNet test dataset split [20], which provides posed RGB frames and dense depth maps (only for analysis). For a 3D scene observed from  $V$  views, we project the encoder features  $\mathbf{F}_v$  from each view into a shared global voxel grid using the ground-truth camera extrinsics and depth. For a specific voxel  $m$  observed in two different views  $v_i$  and  $v_j$ , we extract the corresponding feature vectors  $\mathbf{h}_{m,v_i}$  and  $\mathbf{h}_{m,v_j}$ . The consistency score for this voxel is defined as cosine similarity:

$$S_{\text{voxel}}^{(m)} = \frac{\mathbf{h}_{m,v_i}^\top \mathbf{h}_{m,v_j}}{\|\mathbf{h}_{m,v_i}\| \|\mathbf{h}_{m,v_j}\|}. \quad (3)$$

The final scene-level score is obtained by averaging  $S_{\text{voxel}}^{(m)}$  over all valid voxel pairs across the scene. A higher score indicates that the model implicitly aligns distinct views of the same 3D structure.

**Correlation and Architectural Analysis.** To validate whether this consistency serves as a reliable indicator for downstream 3D capability, we define a Normalized Overall Score (**NOS**). It is calculated by normalizing the performance metrics in Tab. 4 to  $[0, 1]$  with Min-Max normalization across all evaluated models, explicitly including the baseline results to establish a relative performance improvement, and then averaging them into a single scalar.

As illustrated in Fig. 3, plotting the Correspondence Score against NOS reveals a distinct positive correlation, confirming that multi-view consistency is a strong predictor of 3D performance. Furthermore, the results highlight a significant architectural divergence. Models based on UNet architectures (e.g., SVD [4],

Stable Diffusion [61], Vmem [44]) exhibit notably lower consistency scores. We attribute this to the local inductive bias of convolutions and the insufficient scale of data, which limits the receptive field and hinders long-range geometric alignment. In contrast, DiT based models (e.g., Wan2.1 [66]) leverage global attention mechanisms to capture holistic context, achieving remarkably high consistency (> 96%) and consequently superior downstream 3D understanding.

Guided by this evidence, **VEGA-3D** selects DiT-based architectures to provide robust spatial priors. Next, we detail how to actively extract these implicit geometric representations from a frozen generative model.

## 4.2 Video Generative Model as a Latent World Simulator

Building on the premise that generative models encapsulate physical laws, we adopt the pretrained, parameter-frozen Wan2.1-T2V 1.3B [66] as our default generative encoder for its simple text-conditioning interface and strong localization-centric performance. We additionally evaluate other video generative models in Tab. 4, demonstrating that our framework is compatible with different video generative backbones. While traditional visual encoders process raw pixel intensities, video generative models operate in a compressed latent space governed by diffusion dynamics.

Given an input video sequence  $\mathbf{V} \in \mathbb{R}^{T \times H \times W \times 3}$  of  $T$  frames, we first map it to a low-dimensional latent space via the model’s Variational Autoencoder (VAE), yielding  $\mathbf{z}_0 = E(\mathbf{V})$ . However, a static latent representation  $\mathbf{z}_0$  is insufficient to activate the generative model’s reasoning capabilities fully. Diffusion models are trained to enforce structural coherence primarily during active denoising of a corrupted signal; the process of restoration reveals the model’s understanding of structure. Therefore, we perturb the clean latent along the same Flow Matching noising path used by the pretrained backbone. Specifically, we choose a discrete timestep index  $k \in \{0, \dots, K\}$  and define the normalized time as  $t_k = \frac{k}{K}$ . We then sample  $\epsilon \sim \mathcal{N}(\mathbf{0}, \mathbf{I})$  and construct:

$$\mathbf{z}_k = (1 - t_k) \mathbf{z}_0 + t_k \epsilon. \quad (4)$$

We feed  $\mathbf{z}_k$  into the backbone  $\Phi(\cdot)$  using an empty text prompt ( $\mathbf{c}_{\text{text}} = ""$ ). This ensures that the activated features rely solely on the visual signal and the model’s learned physics, minimizing semantic hallucination. We empirically

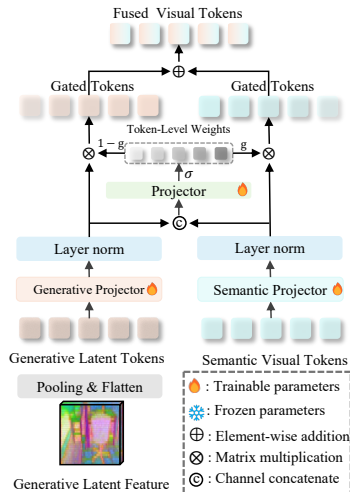


**Fig. 5: Adaptive Gated Fusion.** It dynamically integrates heterogeneous features using a token-level gating mechanism.

select features from the specific intermediate DiT layer  $l$ , as they offer an optimal trade-off between spatial precision and abstract spatiotemporal context:

$$\mathbf{f}_{\text{raw}} = \Phi^{(l)}(\mathbf{z}_k, k; \mathbf{c}_{\text{text}} = ""). \quad (5)$$

After Adaptive Average Pooling to match the semantic tokenization, we obtain the generative representation  $\mathbf{f}_{\text{gen}} \in \mathbb{R}^{T \times N \times D_{\text{gen}}}$ . While this noise-driven process effectively extracts implicit 3D knowledge, these continuous physical features inherently misalign with the MLLM’s discrete semantic space. To bridge this semantic-geometric gap, **VEGA-3D** introduces a tailored fusion strategy.

### 4.3 Bridging the Generative and Semantic Gap

The generative features  $\mathbf{f}_{\text{gen}}$  and semantic features  $\mathbf{f}_{\text{sem}}$  reside in fundamentally different manifolds. To effectively synergize them, we introduce a mechanism to bridge this gap.

As shown in Fig. 5, we first project both streams into the LLM’s hidden dimension  $D_{\text{llm}}$  via independent MLP projectors  $P_{\text{gen}}$  and  $P_{\text{sem}}$ , aligning them to a shared embedding space:

$$\mathbf{F}_{\text{gen}} = P_{\text{gen}}(\mathbf{f}_{\text{gen}}), \mathbf{F}_{\text{sem}} = P_{\text{sem}}(\mathbf{f}_{\text{sem}}). \quad (6)$$

Here,  $\mathbf{F}_{\text{gen}}, \mathbf{F}_{\text{sem}} \in \mathbb{R}^{T \times N \times D_{\text{llm}}}$ , where  $T$  is the number of frames and  $N$  is the number of tokens per frame.

To avoid simply averaging conflicting signals, we employ an **Adaptive Gated Fusion** mechanism. This allows the model to adaptively weigh semantic versus structural cues for each specific token location. For the  $i$ -th spatial token  $\mathbf{F}_i$ , we compute a scalar gate  $g_i \in [0, 1]$ :

$$g_i = \sigma(\mathbf{W}_g^\top \text{Concat}(\text{LN}(\mathbf{F}_{\text{gen},i}), \text{LN}(\mathbf{F}_{\text{sem},i})) + b_g), \quad (7)$$

where  $\sigma(\cdot)$  is the sigmoid function, LN denotes Layer Normalization, and  $\mathbf{W}_g$  is a learnable weight vector. The final fused representation is a convex combination determined by this gate:

$$\mathbf{F}_i^{\text{fused}} = (1 - g_i) \cdot \mathbf{F}_{\text{gen},i} + g_i \cdot \mathbf{F}_{\text{sem},i}. \quad (8)$$

Crucially, this gate  $g_i$  acts as a semantic-geometric arbitrator: it enables the model to prioritize semantic priors for recognition tasks, while dynamically shifting attention to generative world knowledge for tasks requiring spatial reasoning. By seamlessly integrating continuous spatial priors with discrete semantic representations, **VEGA-3D** overcomes the spatial blindness of traditional encoders, achieving dense 3D understanding without explicit geometric supervision.

## 5 Experiments

### 5.1 Implementation Details

We evaluate our framework on three representative axes: (i) **3D scene understanding** on ScanRefer [9], Multi3DRefer [82], Scan2Cap [18], ScanQA [2], and

**Table 1:** Performance comparison on 3D scene understanding benchmarks. Specialists are single-task methods, while generalists target multiple tasks. † indicates the model is trained on extra datasets. Avg. Rank is calculated by averaging the rankings across all available metrics for each method.

Method	Ref.	ScanRefer		Multi3DRefer		Scan2Cap		ScanQA		SQA3D		Avg. Rank
		Acc. <sub>25</sub>	Acc. <sub>5</sub>	F1. <sub>25</sub>	F1. <sub>5</sub>	C. <sub>5</sub>	B-4. <sub>5</sub>	C	EM	EM		
<b>Specialists</b>												
ScanRefer [9]	ECCV 20	37.3	24.3	-	-	-	-	-	-	-	-	16.5
MVT [32]	CVPR 22	40.8	33.3	-	-	-	-	-	-	-	-	15.5
3DVG-Trans [83]	ICCV 21	45.9	34.5	-	-	-	-	-	-	-	-	14.0
ViL3DRel [11]	NeurIPS 21	47.9	37.7	-	-	-	-	-	-	-	-	12.5
M3DRef-CLIP [82]	ICCV 23	51.9	44.7	42.8	-	38.4	-	-	-	-	-	10.2
Scan2Cap [18]	CVPR 21	-	-	-	-	35.2	22.4	-	-	-	-	16.5
ScanQA [2]	CVPR 22	-	-	-	-	-	-	64.9	21.1	47.2	-	12.3
3D-VisTA [92]	ICCV 23	50.6	45.8	-	-	66.9	34.0	69.6	22.4	48.5	-	10.9
<b>Generalists</b>												
Chat-3D [69]	Arxiv 23	-	-	-	-	-	-	53.2	-	-	-	16.0
Chat-3D v2 [30]	Arxiv 23	42.5	38.4	45.1	41.6	63.9	31.8	87.6	-	54.7	-	11.0
LL3DA [12]	CVPR 24	-	-	-	-	62.9	36.0	76.8	-	-	-	12.7
LEO [31]	ICML 24	-	-	-	-	72.4	38.2	101.4	21.5	50.0	-	8.4
Grounded3D-LLM [13]	Arxiv 24	47.9	44.1	45.2	40.6	70.6	35.5	72.7	-	-	-	10.9
PQ3D [93]	ECCV 24	57.0	51.2	-	50.1	80.3	36.0	-	-	47.1	-	8.0
ChatScene [30]	NeurIPS 24	55.5	50.2	57.1	52.4	77.1	36.3	87.7	21.6	54.6	-	7.4
SceneLLM [24]	WACV 25	-	-	-	-	-	-	80.0	27.2	53.6	-	8.3
Inst3D-LLM [77]	CVPR 25	57.8	51.6	58.3	53.5	79.7	38.3	88.6	24.6	-	-	5.5
3D-LLaVA [21]	CVPR 25	51.2	40.6	-	-	78.8	36.9	92.6	-	54.5	-	8.3
3DRS [34]	NeurIPS 25	62.9	56.1	60.4	54.9	<b>86.1</b>	41.6	104.8	30.3	60.6	-	2.2
LLaVA-3D [91]	ICCV25	50.1	42.7	49.8	43.6	84.1	42.6	-	30.6	60.1	-	5.5
LLaVA-4D† [89]	ICLR 26	-	53.2	-	54.3	85.3	<b>45.7</b>	97.8	-	-	-	2.8
Fase3D [54]	CVPR 26	-	-	-	-	78.1	41.3	91.7	-	54.3	-	7.2
Video-3D LLM [87]	CVPR 25	58.1	51.7	58.0	52.7	83.8	41.3	102.1	30.1	58.6	-	4.0
<b>VEGA-3D (Ours)</b>	-	<b>63.2</b>	<b>56.2</b>	<b>60.8</b>	<b>55.1</b>	83.2	42.2	<b>106.3</b>	<b>30.4</b>	<b>61.3</b>	-	<b>1.8</b>

SQA3D [53]; (ii) **spatial reasoning** on VSI-Bench [73] with diverse capability categories and (iii) **robotic manipulation** on LIBERO [48] with four task suites and their average success rate. These benchmarks and reported metrics follow the standard protocols summarized in our main tables.

For 3D scene understanding, we build upon Video-3D LLM [87] as our baseline generalist and select Wan2.1-T2V 1.3B [66] as the latent world simulator plus an adaptive gated fusion module. For VSI-Bench [73], we adopt Qwen2.5VL-7B [58] as the baseline and attach the same plug-and-play generative branch, and the training datasets follow VG-LLM [85]. For LIBERO [48], we start from OpenVLA-OFT [40] and inject generative priors into the visual stream before policy learning. This design keeps the overall training and evaluation pipelines consistent with the corresponding baselines, while isolating the effect of generative priors. More details are provided in **Supplementary**.

For both training and inference, we uniformly sample 32 frames per scan to construct multi-view image sets. The Flow-Matching time interval  $t \in [0, 1]$  is discretized into  $K=1000$  steps in the pretrained Wan2.1 backbone. We denote the discrete timestep index as  $k$  and use  $t_k = \frac{k}{K}$  as the normalized time. By default, we extract features at  $k=300$  (i.e.,  $t_k=0.3$ ) from the 20th DiT layer. When calculating the correspondence score, we use a voxel size of 0.1 for vox-

**Table 2:** The comparison with state-of-the-art models on VSI-Bench. *Spatial-Enhanced Models* are models that are specialized for spatial reasoning. † indicates the baseline model’s performance is finetuned on the same training dataset configurations.

Model	Avg.	Obj. Count	Abs. Dist.	Obj. Size	Room Size	Rel. Dist.	Rel. Dir.	Route Plan	Appr. Order
		Numerical Answer				Multiple-Choice Answer			
<i>Proprietary Models (API)</i>									
GPT-4o [35]	34.0	46.2	5.3	43.8	38.2	37.0	41.3	31.5	28.5
Gemini-1.5-Pro [26]	45.4	56.2	30.9	64.1	43.6	51.3	46.3	36.0	34.6
Gemini-1.5-Flash [26]	42.1	49.8	30.8	53.5	54.4	37.7	41.0	31.5	37.8
<i>Open-source Models</i>									
LongVA-7B [80]	29.2	38.0	16.6	38.9	22.2	33.1	43.3	25.4	15.7
LongVILA-8B [14]	21.6	29.1	9.1	16.7	0.0	29.6	30.7	32.5	25.5
InternVL2-8B [17]	34.6	23.1	28.7	48.2	39.8	36.7	30.7	29.9	39.6
InternVL2-40B [17]	36.0	34.9	26.9	46.5	31.8	42.1	32.2	34.0	39.6
VILA-1.5-40B [52]	31.2	22.4	24.8	48.7	22.7	40.5	25.7	31.5	32.9
LLaVA-OneVision-7B [43]	32.4	47.7	20.2	47.4	12.3	42.5	35.2	29.4	24.4
LLaVA-OneVision-72B [43]	40.2	43.5	23.9	57.6	37.5	42.5	39.9	32.5	44.6
LLaVA-NeXT-Video-7B [49]	35.6	48.5	14.0	47.8	24.2	43.5	42.4	34.0	30.6
LLaVA-NeXT-Video-72B [49]	40.9	48.9	22.8	57.4	35.3	42.4	36.7	35.0	48.6
<i>Spatial-Enhanced Models</i>									
Video-R1-7B [23]	37.1	-	-	-	-	-	-	-	-
vsGRPO-V-7B [45]	40.7	59.9	29.6	50.8	48.3	35.4	35.6	34.0	31.5
SPAR-8B [79]	41.1	-	-	-	-	-	-	-	-
SpaceR-7B [55]	45.6	-	-	-	-	-	-	-	-
3DRS-7B [34]	45.9	68.7	34.8	53.6	56.6	40.9	43.2	30.4	39.2
VG-LLM-4B [86]	45.9	65.6	37.4	54.8	60.2	42.3	46.3	33.0	25.9
VG-LLM-8B [86]	50.1	67.2	38.0	59.3	63.2	47.0	43.9	33.0	49.4
Qwen2.5VL-7B † [58]	48.9	68.3	37.0	57.4	58.7	39.7	43.0	29.4	57.8
<b>VEGA-3D (Ours)</b>	<b>50.5</b>	69.7	35.9	58.0	60.8	45.1	43.1	30.9	60.5

elization. All models are optimized using Adam, with a batch size of 128 and a warm-up ratio of 0.03. The learning rates are set to a maximum of  $1 \times 10^{-5}$  for the language model and  $2 \times 10^{-6}$  for the visual backbone during the warm-up period. We use 8 H100 NVIDIA GPUs for all experiments.

## 5.2 Main Results on 3D Scene Understanding

Tab. 1 reports the main results on five 3D scene understanding benchmarks, covering spatial grounding, dense captioning, and question answering. Overall, our VEGA-3D consistently improves over the Video-3D LLM [87] baseline across most metrics, particularly excelling in localization-centric tasks (e.g., boosting ScanRefer Acc@0.5 from 51.7 to 56.2, SQA3D EM 58.6 to 61.3).

This performance divergence across different tasks suggest an informative pattern about when generative priors help most. We observe notable gains in grounding and spatial QA, where the implicit 3D structural awareness extracted from the generative backbone acts as a robust spatial anchor, which helps reduce the spatial ambiguity of standard MLLMs (see Fig. 2(b)). The slight CIDEr drop in Scan2Cap may indicate a semantic-geometry trade-off: emphasizing structural cues may weaken fine-grained lexical details. Our Adaptive Gated Fusion aims to balance this by token-wise weighting between the two streams.

Notably, in contrast to prevailing state-of-the-art methods that rely on heavy geometric supervision [34] via external 3D teachers [68] or curated 3D-heavy

datasets [89], our improvements are achieved entirely without explicit 3D annotations. This conveys a powerful insight: large-scale video generation models, through the pretext of temporal synthesis, have already internalized a robust 3D world model from the vast causality of the natural world. By repurposing these models as Latent World Simulators, we bypass the data-scarcity bottleneck posed by 3D-specific labels. This framework offers a highly scalable, data-efficient paradigm, demonstrating that the next frontier for 3D spatial awareness in MLLMs may not lie in more 3D data but in unleashing the latent physical priors already dormant within generative foundations.

### 5.3 Generalization to Spatial Reasoning and Manipulation

To validate the generalization ability of VEGA-3D, we extend our evaluation to 3D visual-spatial reasoning and embodied manipulation.

**Spatial reasoning on VSI-Bench.** Tab. 2 evaluates spatial reasoning on VSI-Bench [73], a comprehensive benchmark designed to diagnose diverse visual-spatial skills from videos, such as relative distance and route planning. By seamlessly augmenting the Qwen2.5VL-7B [58] baseline with our generative priors, we observe consistent gains across the overall average and multiple sub-categories. This trend aligns with the recent emphasis on geometry-aware mechanisms for spatial reasoning, yet our method remains lightweight and plug-and-play.

**Table 3:** The comparison of the simulation robotic manipulation benchmark LIBERO, the performance is evaluated with the average success rate SR (%)

Method	Reference	Spatial	Object	Goal	Long	Avg.
Diffusion Policy [19]	ICRR 23	78.3	92.5	68.3	50.5	72.4
Octo [63]	RSS 24	78.9	85.7	84.6	51.1	75.1
OpenVLA [41]	CoRL 24	84.7	88.4	79.2	53.7	76.5
DiT Policy [29]	ICCV 25	84.2	96.3	85.4	63.8	82.4
CoT-VLA [84]	CVPR 25	87.5	91.6	87.6	69.0	81.1
UniVLA [6]	RSS 25	96.5	96.8	95.6	92.0	95.2
OpenVLA-OFT [40]	RSS 25	<b>97.5</b>	<b>98.3</b>	<b>97.8</b>	<b>94.4</b>	<b>97.0</b>
<b>VEGA-3D (Ours)</b>	-	<b>97.4</b>	<b>99.4</b>	<b>97.0</b>	<b>95.2</b>	<b>97.3</b>

**Robotic manipulation on LIBERO.** Beyond passive reasoning, we assess whether our generative priors can ground active physical agents. Tab. 3 reports success rates on the LIBERO [48] suite, a challenging simulation benchmark for robotic manipulation. We inject our **VEGA-3D** generative priors into the visual stream of a pre-trained Vision-Language-Action (VLA) model (e.g., OpenVLA-OFT [40]) prior to policy learning. Despite being extracted without explicit action-conditioned training, the generative features further enhance the already highly saturated baseline performance. Notably, we observe specific breakthroughs in handling complex object interactions and long-horizon tasks. This suggests that the spatial regularities and physical knowledge embedded within the Latent World Simulator are directly transferable, providing exceptional robustness and effectively guiding the VLA’s planning and action execution in demanding scenarios.

**Table 4:** Experiments on using different discriminative and generative foundation models. Bold denotes the best in each group.

Models	Params	ScanRefer		Multi3DRefer		Scan2Cap		ScanQA		SQA3D
		Acc. <sub>25</sub>	Acc. <sub>5</sub>	F1. <sub>25</sub>	F1. <sub>5</sub>	C. <sub>5</sub>	B-4.5	C	EM	EM
Baseline	-	58.1	51.7	58.0	52.7	83.8	41.3	102.1	30.1	58.6
<i>Discriminative Models</i>										
V-JEPA v2 [1]	1B	61.7	54.9	60.2	54.7	79.8	41.5	106.6	30.7	61.2
DinoV3-Large [62]	0.3B	61.1	54.2	59.6	54.1	80.6	41.1	105.9	30.5	61.9
VGGT [68]	1.1B	62.3	55.3	60.1	54.5	82.8	42.0	105.8	30.5	61.4
<i>Generative Models</i>										
Stable Video Diffusion [4]	1.5B	61.3	54.8	59.9	54.6	80.9	41.9	105.1	30.1	61.3
Stable Diffusion 2.1 [61]	0.9B	62.1	55.1	60.3	54.9	83.0	42.0	106.8	30.4	60.6
Vmem [44]	1.3B	62.5	55.7	60.2	54.7	82.0	41.9	106.0	30.0	61.4
SEVA [90]	1.3B	62.3	55.5	60.1	54.5	82.5	42.1	107.6	30.8	60.9
VAE [61]	0.08B	62.0	55.1	60.3	54.8	83.7	42.3	106.0	30.5	61.4
Wan2.1-VACE [37]	1.3B	62.2	55.3	60.3	55.0	82.8	42.7	107.8	31.0	61.8
Wan2.1-T2V [66]	1.3B	63.2	56.2	60.8	55.1	83.2	42.2	106.3	30.4	61.3

5.4 Ablation Studies

To validate our design choices, we conduct comprehensive ablation studies using Wan2.1-T2V 1.3B as the default generative encoder. We note that Wan2.1-VACE can achieve higher QA scores in Tab. 4, while T2V provides stronger grounding-oriented performance; thus, we keep T2V as the default encoder.

**Generative vs. Discriminative Priors.**

Tab. 4 and Fig. 3(b) reveal a strong positive correlation between multi-view consistency and 3D scene understanding. While traditional discriminative models (e.g., DINO V3 [62], V-JEPA v2 [1], SigLIP [78]) offer rich semantics, they lack explicit 3D consistency. Conversely, DiT-based generative models and 3D foundation model like VGGT [68] excel at capturing robust spatial priors. DiTs significantly outperform UNet-based models, as their global attention mechanisms preserve long-range geometric dependencies better than local convolutions. This confirms that video generation models provide superior 3D prior for spatial reasoning compared to standard visual learners.

**Dynamics of Internal Representations: Noise Levels and Layers.**

The generative prior varies significantly across the diffusion process and network depth (Fig. 6). **(i) Noise Ratio  $t_k$ :** Performance peaks at intermediate noise level. Clean latents underutilize the model’s denoising capabilities, while excessive noise destroys structural signals. Moderate noise optimally forces the model to engage its learned physics to restore underlying 3D structures. **(ii) Layer Selection:** Intermediate layers provide the optimal abstraction for spa-

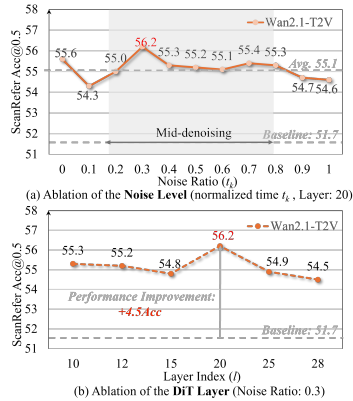


**Fig. 6: Ablation studies on noise injection and DiT depth.** (a) Performance peaks at intermediate noise levels. (b) Specific intermediate layers capture the most robust geometric cues.

**Table 5:** Ablation study of the effects of different feature fusion modules. All models are finetuned with the same training data and built on Wan2.1-T2V 1.3B at sampling step  $k = 300$  and the 20th layer feature.

Type	ScanRefer		Multi3DRefer		Scan2Cap		ScanQA		SQA3D
	Acc.25	Acc.5	F1.25	F1.5	C.5	B-4.5	C	EM	EM
Baseline	58.1	51.7	58.0	52.7	<b>83.8</b>	41.3	102.1	30.1	58.6
Only generative features	54.9	48.3	53.7	48.6	25.2	30.0	74.0	21.1	52.0
Add	61.5	54.6	59.6	54.1	81.4	41.6	<b>106.3</b>	<b>30.4</b>	<b>61.8</b>
Channel Concat+MLP	55.1	48.9	53.6	48.7	33.2	31.8	81.6	22.9	52.3
Sequence Concat	59.5	53.0	58.4	53.2	79.4	41.0	104.7	30.2	61.5
Cross-Attn (1 Layer)	58.5	51.9	57.9	52.6	48.8	34.7	104.9	29.6	61.0
Cross-Attn (3 Layers)	58.0	51.5	57.5	52.1	47.8	34.8	102.2	29.2	60.5
Channel-Level-Gated	61.8	54.9	60.0	54.4	82.2	41.9	105.7	30.3	61.2
Adaptive-Gated-Fusion(Ours)	<b>63.2</b>	<b>56.2</b>	<b>60.8</b>	<b>55.1</b>	83.2	<b>42.2</b>	<b>106.3</b>	<b>30.4</b>	61.3

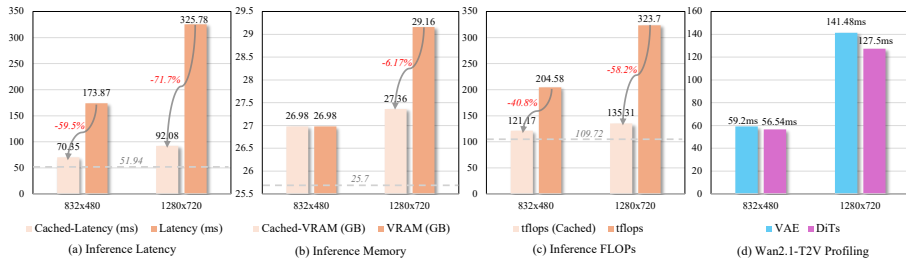


**Fig. 7: Inference overhead** We cache the **Wan2.1-T2V** features once per scene and reuse them for all questions, substantially reducing inference overhead. The gray dashed line indicates the baseline result without the generative branch.

tial reasoning, effectively balancing the low-level textures of early layers and the pixel-level rendering of deeper layers.

**Effectiveness of Adaptive Gated Fusion.** Tab. 5 demonstrates the necessity of our Adaptive Gated Fusion. Relying solely on generative features causes a substantial performance drop, confirming that generative priors complement rather than replace semantic representations. Among lightweight fusion variants, our method achieves the best overall trade-off: it outperforms other fusion baselines on most metrics, and matches the best results on ScanQA (C/EM). We note that a naive Add operation attains a slightly higher SQA3D EM (61.8 vs. 61.3), but it is consistently weaker on grounding and captioning metrics, suggesting that a fixed, non-adaptive fusion weight cannot reliably resolve the semantic-geometric distribution gap. In contrast, our token-level gating dynamically balances semantic and geometric priors, yielding more consistent gains across diverse tasks.

## 6 Conclusion

We introduce **VEGA-3D**, a plug-and-play framework that repurposes modern video generation models as *Latent World Simulators* to mitigate the spatial blindness of MLLMs. By activating these priors via noise injection and aligning them with semantic tokens through *Adaptive Gated Fusion*, VEGA-3D injects dense geometric anchors into MLLMs, consistently improving scene understanding, spatial reasoning, and manipulation *without* extra 3D supervision.

**Limitations and Future Work.** Incorporating a video diffusion backbone increases inference cost (Fig. 7). Nevertheless, it delivers substantial and consistent performance gains, making the trade-off acceptable in practice. Future work will distill these priors into lightweight encoders and extend the framework to more dynamic scene understanding.

## References

- [1] Assran, M., Bardes, A., Fan, D., Garrido, Q., Howes, R., Muckley, M., Rizvi, A., Roberts, C., Sinha, K., Zholus, A., et al.: V-jepa 2: Self-supervised video models enable understanding, prediction and planning. arXiv preprint arXiv:2506.09985 (2025) 6, 13, 25, 27
- [2] Azuma, D., Miyanishi, T., Kurita, S., Kawanabe, M.: Scanqa: 3d question answering for spatial scene understanding. In: Proc. IEEE Conf. Comput. Vis. Pattern Recognit. (2022), license: Creative Commons Attribution-NonCommercial-ShareAlike 3.0 Unported License 9, 10, 24
- [3] Ball, P.J., Bauer, J., Belletti, F., Brownfield, B., Ephrat, A., Fruchter, S., Gupta, A., Holsheimer, K., Holynski, A., Hron, J., Kaplanis, C., Limont, M., McGill, M., Oliveira, Y., Parker-Holder, J., Perbet, F., Scully, G., Shar, J., Spencer, S., Tov, O., Villegas, R., Wang, E., Yung, J., Baetu, C., Berbel, J., Bridson, D., Bruce, J., Buttimore, G., Chakera, S., Chandra, B., Collins, P., Cullum, A., Damoc, B., Dasagi, V., Gazeau, M., Gbadamosi, C., Han, W., Hirst, E., Kachra, A., Kerley, L., Kjems, K., Knoepfel, E., Koriakin, V., Lo, J., Lu, C., Mehring, Z., Moufarek, A., Nandwani, H., Oliveira, V., Pardo, F., Park, J., Pierson, A., Poole, B., Ran, H., Salimans, T., Sanchez, M., Saprykin, I., Shen, A., Sidhwani, S., Smith, D., Stanton, J., Tomlinson, H., Vijaykumar, D., Wang, L., Wingfield, P., Wong, N., Xu, K., Yew, C., Young, N., Zubov, V., Eck, D., Erhan, D., Kavukcuoglu, K., Hassabis, D., Gharamani, Z., Hadsell, R., van den Oord, A., Mosseri, I., Bolton, A., Singh, S., Rocktäschel, T.: Genie 3: A new frontier for world models (2025) 2, 5
- [4] Blattmann, A., Dockhorn, T., Kulal, S., Mendelevitch, D., Kilian, M., Lorenz, D., Levi, Y., English, Z., Voleti, V., Letts, A., et al.: Stable video diffusion: Scaling latent video diffusion models to large datasets. arXiv preprint arXiv:2311.15127 (2023) 7, 13, 25, 27
- [5] Brooks, T., Peebles, B., Holmes, C., DePue, W., Guo, Y., Jing, L., Schnurr, D., Taylor, J., Luhman, T., Luhman, E., Ng, C., Wang, R., Ramesh, A.: Video generation models as world simulators (2024), <https://openai.com/research/video-generation-models-as-world-simulators> 5
- [6] Bu, Q., Yang, Y., Cai, J., Gao, S., Ren, G., Yao, M., Luo, P., Li, H.: Univla: Learning to act anywhere with task-centric latent actions. Robotics: Science and Systems (RSS) (2025) 12
- [7] Cheang, C.L., Chen, G., Jing, Y., Kong, T., Li, H., Li, Y., Liu, Y., Wu, H., Xu, J., Yang, Y., et al.: Gr-2: A generative video-language-action model with web-scale knowledge for robot manipulation. arXiv preprint arXiv:2410.06158 (2024) 2

- [8] Chen, B., Xu, Z., Kirmani, S., Ichter, B., Sadigh, D., Guibas, L., Xia, F.: Spatialvlm: Endowing vision-language models with spatial reasoning capabilities. In: Proc. IEEE Conf. Comput. Vis. Pattern Recognit. pp. 14455–14465 (2024) [5](#)
- [9] Chen, D.Z., Chang, A.X., Nießner, M.: Scanrefer: 3d object localization in rgb-d scans using natural language. In: Proc. Eur. Conf. Comput. Vis. (2020), license: Creative Commons Attribution-NonCommercial-ShareAlike 3.0 Unported License [9](#), [10](#), [24](#)
- [10] Chen, D., Shukor, M., Moutakanni, T., Chung, W., Yu, J., Kasarla, T., Bolourchi, A., LeCun, Y., Fung, P.: Vl-jepa: Joint embedding predictive architecture for vision-language. In: Proc. Int. Conf. Learn. Representations (2026) [6](#)
- [11] Chen, S., Guhur, P., Tapaswi, M., Schmid, C., Laptev, I.: Language conditioned spatial relation reasoning for 3d object grounding. In: Proc. Adv. Neural Inf. Process. Syst. (2022) [10](#)
- [12] Chen, S., Chen, X., Zhang, C., Li, M., Yu, G., Fei, H., Zhu, H., Fan, J., Chen, T.: LL3DA: visual interactive instruction tuning for omni-3d understanding, reasoning, and planning. In: Proc. IEEE Conf. Comput. Vis. Pattern Recognit. (2024) [10](#)
- [13] Chen, Y., Yang, S., Huang, H., Wang, T., Xu, R., Lyu, R., Lin, D., Pang, J.: Grounded 3d-llm with referent tokens. arXiv preprint arXiv:2405.10370 (2024) [10](#)
- [14] Chen, Y., Xue, F., Li, D., Hu, Q., Zhu, L., Li, X., Fang, Y., Tang, H., Yang, S., Liu, Z., et al.: Longvila: Scaling long-context visual language models for long videos. arXiv preprint arXiv:2408.10188 (2024) [11](#)
- [15] Chen, Z., Zhang, X., Xu, H., Xie, J., Tu, Z.: Cvp: Central-peripheral vision-inspired multimodal model for spatial reasoning. arXiv preprint arXiv:2512.08135 (2025) [5](#)
- [16] Chen, Z., Zhang, M., Yu, X., Luo, X., Sun, M., Pan, Z., Feng, Y., Pei, P., Cai, X., Huang, R.: Think with 3d: Geometric imagination grounded spatial reasoning from limited views. arXiv preprint arXiv:2510.18632 (2025) [2](#), [4](#)
- [17] Chen, Z., Wang, W., Tian, H., Ye, S., Gao, Z., Cui, E., Tong, W., Hu, K., Luo, J., Ma, Z., et al.: How far are we to gpt-4v? closing the gap to commercial multimodal models with open-source suites. Science China Information Sciences **67**(12), 220101 (2024) [11](#)
- [18] Chen, Z., Gholami, A., Nießner, M., Chang, A.X.: Scan2cap: Context-aware dense captioning in rgb-d scans. In: Proc. IEEE Conf. Comput. Vis. Pattern Recognit. (2021), license: Creative Commons Attribution-NonCommercial-ShareAlike 3.0 Unported License [9](#), [10](#), [24](#)
- [19] Chi, C., Xu, Z., Feng, S., Cousineau, E., Du, Y., Burchfiel, B., Tedrake, R., Song, S.: Diffusion policy: Visuomotor policy learning via action diffusion. The International Journal of Robotics Research (2023) [12](#)
- [20] Dai, A., Chang, A.X., Savva, M., Halber, M., Funkhouser, T., Nießner, M.: Scannet: Richly-annotated 3d reconstructions of indoor scenes. In: Proc. IEEE Conf. Comput. Vis. Pattern Recognit. (2017), license: ScanNet Terms of Use [7](#), [24](#)

- [21] Deng, J., He, T., Jiang, L., Wang, T., Dayoub, F., Reid, I.: 3d-llava: Towards generalist 3d llms with omni superpoint transformer. In: Proc. IEEE Conf. Comput. Vis. Pattern Recognit. (2025) [10](#)
- [22] Fan, Z., Zhang, J., Li, R., Zhang, J., Chen, R., Hu, H., Wang, K., Qu, H., Wang, D., Yan, Z., et al.: Vlm-3r: Vision-language models augmented with instruction-aligned 3d reconstruction. In: Proc. IEEE Conf. Comput. Vis. Pattern Recognit. (2026) [5](#), [24](#)
- [23] Feng, K., Gong, K., Li, B., Guo, Z., Wang, Y., Peng, T., Wu, J., Zhang, X., Wang, B., Yue, X.: Video-r1: Reinforcing video reasoning in mllms. In: Proc. Adv. Neural Inf. Process. Syst. (2025) [11](#)
- [24] Fu, R., Liu, J., Chen, X., Nie, Y., Xiong, W.: Scene-llm: Extending language model for 3d visual reasoning. In: Proceedings of the Winter Conference on Applications of Computer Vision (WACV). pp. 2195–2206 (February 2025) [10](#)
- [25] Gao, J., Sarkar, B., Xia, F., Xiao, T., Wu, J., Ichter, B., Majumdar, A., Sadigh, D.: Physically grounded vision-language models for robotic manipulation. In: Proc. IEEE Int. Conf. Robotics Automation. pp. 12462–12469. IEEE (2024) [2](#)
- [26] Gemini Team: Gemini 1.5: Unlocking multimodal understanding across millions of tokens of context. arXiv preprint arXiv:2403.05530 (2024) [11](#)
- [27] Guo, Z., Zhang, R., Zhu, X., Tang, Y., Ma, X., Han, J., Chen, K., Gao, P., Li, X., Li, H., et al.: Point-bind & point-llm: Aligning point cloud with multi-modality for 3d understanding, generation, and instruction following. arXiv preprint arXiv:2309.00615 (2023) [2](#), [4](#)
- [28] Hong, W., Ding, M., Zheng, W., Liu, X., Tang, J.: Cogvideo: Large-scale pretraining for text-to-video generation via transformers. In: Proc. Int. Conf. Learn. Representations (2023) [5](#)
- [29] Hou, Z., Zhang, T., Xiong, Y., Duan, H., Pu, H., Tong, R., Zhao, C., Zhu, X., Qiao, Y., Dai, J., et al.: Dita: Scaling diffusion transformer for generalist vision-language-action policy. In: Proc. IEEE Int. Conf. Comput. Vis. pp. 7686–7697 (2025) [12](#)
- [30] Huang, H., Wang, Z., Huang, R., Liu, L., Cheng, X., Zhao, Y., Jin, T., Zhao, Z.: Chat-3d v2: Bridging 3d scene and large language models with object identifiers. CoRR (2023) [4](#), [10](#)
- [31] Huang, J., Yong, S., Ma, X., Linghu, X., Li, P., Wang, Y., Li, Q., Zhu, S., Jia, B., Huang, S.: An embodied generalist agent in 3d world. In: Proc. Int. Conf. Mach. Learn. (2024) [10](#)
- [32] Huang, S., Chen, Y., Jia, J., Wang, L.: Multi-view transformer for 3d visual grounding. In: Proc. IEEE Conf. Comput. Vis. Pattern Recognit. (2022) [10](#)
- [33] Huang, S., Wu, J., Zhou, Q., Miao, S., Long, M.: Vid2world: Crafting video diffusion models to interactive world models. In: Proc. Int. Conf. Learn. Representations (2026) [2](#)
- [34] Huang, X., Wu, J., Xie, Q., Han, K.: 3drs: Mllms need 3d-aware representation supervision for scene understanding. In: Proc. Adv. Neural Inf. Process. Syst. (2025) [2](#), [4](#), [10](#), [11](#)

- [35] Hurst, A., Lerer, A., Goucher, A.P., Perelman, A., Ramesh, A., Clark, A., Ostrow, A., Welihinda, A., Hayes, A., Radford, A., et al.: Gpt-4o system card. arXiv preprint arXiv:2410.21276 (2024) [11](#)
- [36] Jia, M., Qi, Z., Zhang, S., Zhang, W., Yu, X., He, J., Wang, H., Yi, L.: Omnispatial: Towards comprehensive spatial reasoning benchmark for vision language models. In: Proc. Int. Conf. Learn. Representations (2026) [5](#)
- [37] Jiang, Z., Han, Z., Mao, C., Zhang, J., Pan, Y., Liu, Y.: Vace: All-in-one video creation and editing. In: Proc. IEEE Int. Conf. Comput. Vis. pp. 17191–17202 (2025) [2](#), [13](#), [25](#), [27](#)
- [38] Kang, B., Yue, Y., Lu, R., Lin, Z., Zhao, Y., Wang, K., Huang, G., Feng, J.: How far is video generation from world model: A physical law perspective. In: Proc. Int. Conf. Mach. Learn. (2025) [2](#)
- [39] Kim, G., Han, J., Cho, S.: Videofrom3d: 3d scene video generation via complementary image and video diffusion models. In: Proceedings of the SIGGRAPH Asia 2025 Conference Papers. pp. 1–11 (2025) [2](#)
- [40] Kim, M.J., Finn, C., Liang, P.: Fine-tuning vision-language-action models: Optimizing speed and success. Robotics: Science and Systems (RSS) (2025) [10](#), [12](#), [24](#)
- [41] Kim, M.J., Pertsch, K., Karamcheti, S., Xiao, T., Balakrishna, A., Nair, S., Rafailov, R., Foster, E., Lam, G., Sanketi, P., et al.: Openvla: An open-source vision-language-action model. In: Proceedings of the 8th Conference on Robot Learning. pp. 2679–2713. PMLR (2024) [12](#)
- [42] Kondratyuk, D., Yu, L., Gu, X., Lezama, J., Huang, J., Schindler, G., Hornung, R., Birodkar, V., Yan, J., Chiu, M.C., et al.: Videopoet: A large language model for zero-shot video generation. arXiv preprint arXiv:2312.14125 (2023) [5](#)
- [43] Li, B., Zhang, Y., Guo, D., Zhang, R., Li, F., Zhang, H., Zhang, K., Zhang, P., Li, Y., Liu, Z., et al.: Llava-onevision: Easy visual task transfer. arXiv preprint arXiv:2408.03326 (2024) [11](#)
- [44] Li, R., Torr, P., Vedaldi, A., Jakab, T.: Vmem: Consistent interactive video scene generation with surfel-indexed view memory. arXiv preprint arXiv:2506.18903 (2025) [2](#), [3](#), [5](#), [8](#), [13](#), [25](#), [27](#), [28](#)
- [45] Liao, Z., Xie, Q., Zhang, Y., Kong, Z., Lu, H., Yang, Z., Deng, Z.: Improved visual-spatial reasoning via rl-zero-like training. arXiv preprint arXiv:2504.00883 (2025) [11](#)
- [46] Lin, J., Zhu, C., Xu, R., Mao, X., Liu, X., Wang, T., Pang, J.: Ost-bench: Evaluating the capabilities of mllms in online spatio-temporal scene understanding. arXiv preprint arXiv:2507.07984 (2025) [5](#)
- [47] Lipman, Y., Chen, R.T., Ben-Hamu, H., Nickel, M., Le, M.: Flow matching for generative modeling. arXiv preprint arXiv:2210.02747 (2022) [6](#)
- [48] Liu, B., Zhu, Y., Gao, C., Feng, Y., Liu, Q., Zhu, Y., Stone, P.: Libero: Benchmarking knowledge transfer for lifelong robot learning. Advances in Neural Information Processing Systems **36** (2024) [3](#), [10](#), [12](#), [24](#)
- [49] Liu, H., Li, C., Li, Y., Li, B., Zhang, Y., Shen, S., Lee, Y.J.: Llava-next: Improved reasoning, ocr, and world knowledge (January 2024), <https://llava-vl.github.io/blog/2024-01-30-llava-next/> [11](#)

- [50] Liu, H., Li, C., Wu, Q., Lee, Y.J.: Visual instruction tuning. *Advances in neural information processing systems* **36**, 34892–34916 (2023) [5](#)
- [51] Liu, Y., Liu, L., Zheng, Y., Liu, Y., Dang, F., Li, N., Ma, K.: Embodied navigation. *Science China Information Sciences* **68**(4), 1–39 (2025) [2](#)
- [52] Liu, Z., Zhu, L., Shi, B., Zhang, Z., Lou, Y., Yang, S., Xi, H., Cao, S., Gu, Y., Li, D., et al.: Nvila: Efficient frontier visual language models. In: *Proc. IEEE Conf. Comput. Vis. Pattern Recognit.* pp. 4122–4134 (2025) [11](#)
- [53] Ma, X., Yong, S., Zheng, Z., Li, Q., Liang, Y., Zhu, S., Huang, S.: SQA3D: situated question answering in 3d scenes. In: *Proc. Int. Conf. Learn. Representations (2023)*, license: CC-BY-4.0 [10](#), [24](#)
- [54] Mei, G., Lin, W., Riz, L., Wu, Y., Wang, Y., Poiesi, F.: Efficient encoder-free fourier-based 3d large multimodal model. In: *Proc. IEEE Conf. Comput. Vis. Pattern Recognit.* (2026) [10](#)
- [55] Ouyang, K., Liu, Y., Wu, H., Liu, Y., Zhou, H., Zhou, J., Meng, F., Sun, X.: Spacer: Reinforcing mllms in video spatial reasoning. *arXiv preprint arXiv:2504.01805* (2025) [11](#)
- [56] Qi, Z., Fang, Y., Sun, Z., Wu, X., Wu, T., Wang, J., Lin, D., Zhao, H.: Gpt4point: A unified framework for point-language understanding and generation. In: *Proc. IEEE Conf. Comput. Vis. Pattern Recognit.* (2024) [2](#), [4](#)
- [57] Qi, Z., Zhang, Z., Fang, Y., Wang, J., Zhao, H.: Gpt4scene: Understand 3d scenes from videos with vision-language models. In: *Proc. Int. Conf. Learn. Representations (2026)* [4](#)
- [58] Qwen Team: Qwen2.5-vl technical report. *arXiv preprint arXiv:2502.13923* (2025) [10](#), [11](#), [12](#)
- [59] Radford, A., Kim, J.W., Hallacy, C., Ramesh, A., Goh, G., Agarwal, S., Sastry, G., Askell, A., Mishkin, P., Clark, J., et al.: Learning transferable visual models from natural language supervision. In: *Proc. Int. Conf. Mach. Learn.* pp. 8748–8763. PMLR (2021) [5](#)
- [60] Ren, X., Shen, T., Huang, J., Ling, H., Lu, Y., Nimier-David, M., Müller, T., Keller, A., Fidler, S., Gao, J.: Gen3c: 3d-informed world-consistent video generation with precise camera control. In: *Proceedings of the Computer Vision and Pattern Recognition Conference.* pp. 6121–6132 (2025) [2](#), [5](#)
- [61] Rombach, R., Blattmann, A., Lorenz, D., Esser, P., Ommer, B.: High-resolution image synthesis with latent diffusion models. In: *Proc. IEEE Conf. Comput. Vis. Pattern Recognit.* pp. 10684–10695 (2022) [8](#), [13](#), [25](#), [27](#)
- [62] Siméoni, O., Vo, H.V., Seitzer, M., Baldassarre, F., Oquab, M., Jose, C., Khalidov, V., Szafraniec, M., Yi, S., Ramamonjisoa, M., et al.: Dinov3. *arXiv preprint arXiv:2508.10104* (2025) [13](#), [25](#), [27](#)
- [63] Team, O.M., Ghosh, D., Walke, H., Pertsch, K., Black, K., Mees, O., Dasari, S., Hejna, J., Kreiman, T., Xu, C., et al.: Octo: An open-source generalist robot policy. *Robotics: Science and Systems (RSS)* (2024) [12](#)
- [64] Tschannen, M., Gritsenko, A., Wang, X., Naeem, M.F., Alabdulmohsin, I., Parthasarathy, N., Evans, T., Beyer, L., Xia, Y., Mustafa, B., et al.: Siglip 2: Multilingual vision-language encoders with improved semantic understanding, localization, and dense features. *arXiv preprint arXiv:2502.14786* (2025) [2](#)

- [65] Valevski, D., Leviathan, Y., Arar, M., Fruchter, S.: Diffusion models are real-time game engines. In: Proc. Int. Conf. Learn. Representations (2025) [2](#)
- [66] Wan, T., Wang, A., Ai, B., Wen, B., Mao, C., Xie, C.W., Chen, D., Yu, F., Zhao, H., Yang, J., et al.: Wan: Open and advanced large-scale video generative models. arXiv preprint arXiv:2503.20314 (2025) [2](#), [5](#), [6](#), [7](#), [8](#), [10](#), [13](#), [25](#), [27](#)
- [67] Wang, H., Zhao, Y., Wang, T., Fan, H., Zhang, X., Zhang, Z.: Ross3d: Reconstructive visual instruction tuning with 3d-awareness. In: Proc. IEEE Int. Conf. Comput. Vis. (2025) [2](#), [4](#)
- [68] Wang, J., Chen, M., Karaev, N., Vedaldi, A., Rupprecht, C., Novotny, D.: Vggt: Visual geometry grounded transformer. In: Proc. IEEE Conf. Comput. Vis. Pattern Recognit. pp. 5294–5306 (2025) [11](#), [13](#), [25](#), [27](#)
- [69] Wang, Z., Huang, H., Zhao, Y., Zhang, Z., Zhao, Z.: Chat-3d: Data-efficiently tuning large language model for universal dialogue of 3d scenes. arXiv preprint arXiv:2308.08769 (2023) [10](#)
- [70] Xiao, Z., Lan, Y., Zhou, Y., Ouyang, W., Yang, S., Zeng, Y., Pan, X.: Worldmem: Long-term consistent world simulation with memory. In: Proc. Adv. Neural Inf. Process. Syst. (2025) [2](#)
- [71] Xu, R., Wang, X., Wang, T., Chen, Y., Pang, J., Lin, D.: Pointllm: Empowering large language models to understand point clouds. In: Proc. Eur. Conf. Comput. Vis. (2024) [2](#), [4](#)
- [72] Xu, W., Shi, C., Tu, S., Zhou, X., Liang, D., Bai, X.: A unified framework for 3d scene understanding. *Advances in Neural Information Processing Systems* **37**, 59468–59490 (2024) [2](#)
- [73] Yang, J., Yang, S., Gupta, A.W., Han, R., Fei-Fei, L., Xie, S.: Thinking in space: How multimodal large language models see, remember, and recall spaces. In: Proc. IEEE Conf. Comput. Vis. Pattern Recognit. pp. 10632–10643 (2025) [3](#), [5](#), [10](#), [12](#)
- [74] Yang, S., Xu, R., Xie, Y., Yang, S., Li, M., Lin, J., Zhu, C., Chen, X., Duan, H., Yue, X., et al.: Mmsi-bench: A benchmark for multi-image spatial intelligence. In: Proc. Int. Conf. Learn. Representations (2026) [5](#)
- [75] Yang, Z., Teng, J., Zheng, W., Ding, M., Huang, S., Xu, J., Yang, Y., Hong, W., Zhang, X., Feng, G., et al.: Cogvideox: Text-to-video diffusion models with an expert transformer. In: Proc. Int. Conf. Learn. Representations (2025) [5](#)
- [76] Yin, B., Wang, Q., Zhang, P., Zhang, J., Wang, K., Wang, Z., Zhang, J., Chandrasegaran, K., Liu, H., Krishna, R., et al.: Spatial mental modeling from limited views. In: Structural Priors for Vision Workshop at ICCV'25 (2025) [5](#)
- [77] Yu, H., Li, W., Wang, S., Chen, J., Zhu, J.: Inst3d-lmm: Instance-aware 3d scene understanding with multi-modal instruction tuning. In: Proc. IEEE Conf. Comput. Vis. Pattern Recognit. (2025) [2](#), [10](#)
- [78] Zhai, X., Mustafa, B., Kolesnikov, A., Beyer, L.: Sigmoid loss for language image pre-training. In: Proceedings of the IEEE/CVF International Conference on Computer Vision. pp. 11975–11986 (2023) [2](#), [5](#), [7](#), [13](#)

- [79] Zhang, J., Chen, Y., Zhou, Y., Xu, Y., Huang, Z., Mei, J., Chen, J., Yuan, Y.J., Cai, X., Huang, G., et al.: From flatland to space: Teaching vision-language models to perceive and reason in 3d. In: Proc. IEEE Int. Conf. Comput. Vis. (2025) [11](#)
- [80] Zhang, P., Zhang, K., Li, B., Zeng, G., Yang, J., Zhang, Y., Wang, Z., Tan, H., Li, C., Liu, Z.: Long context transfer from language to vision. arXiv preprint arXiv:2406.16852 (2024) [11](#)
- [81] Zhang, W., Ng, W.E., Ma, L., Wang, Y., Zhao, J., Koenecke, A., Li, B., Wanglu, W.: Sphere: Unveiling spatial blind spots in vision-language models through hierarchical evaluation. In: Proc. Annual Meeting of the Association for Computational Linguistics. pp. 11591–11609 (2025) [5](#)
- [82] Zhang, Y., Gong, Z., Chang, A.X.: Multi3drefer: Grounding text description to multiple 3d objects. In: Proc. IEEE Int. Conf. Comput. Vis. (2023), license: MIT [9](#), [10](#), [24](#)
- [83] Zhao, L., Cai, D., Sheng, L., Xu, D.: 3dvg-transformer: Relation modeling for visual grounding on point clouds. In: Proc. IEEE Int. Conf. Comput. Vis. (2021) [10](#)
- [84] Zhao, Q., Lu, Y., Kim, M.J., Fu, Z., Zhang, Z., Wu, Y., Li, Z., Ma, Q., Han, S., Finn, C., Handa, A., Liu, M.Y., Xiang, D., Wetzstein, G., Lin, T.Y.: Cot-vla: Visual chain-of-thought reasoning for vision-language-action models. In: Proc. IEEE Conf. Comput. Vis. Pattern Recognit. pp. 1702–1713 (2025) [12](#)
- [85] Zheng, D., Huang, S., Li, Y., Wang, L.: Learning from videos for 3d world: Enhancing mllms with 3d vision geometry priors. In: Proc. Adv. Neural Inf. Process. Syst. (2025) [10](#)
- [86] Zheng, D., Huang, S., Li, Y., Wang, L.: Learning from videos for 3d world: Enhancing mllms with 3d vision geometry priors. In: Proc. Adv. Neural Inf. Process. Syst. (2025) [11](#), [24](#)
- [87] Zheng, D., Huang, S., Wang, L.: Video-3d llm: Learning position-aware video representation for 3d scene understanding. In: Proc. IEEE Conf. Comput. Vis. Pattern Recognit. (2025) [2](#), [4](#), [10](#), [11](#), [24](#)
- [88] Zheng, D., Huang, S., Zhao, L., Zhong, Y., Wang, L.: Towards learning a generalist model for embodied navigation. In: Proc. IEEE Conf. Comput. Vis. Pattern Recognit. pp. 13624–13634 (2024) [2](#)
- [89] Zhou, H., Lee, G.H.: Llava-4d: Embedding spatiotemporal prompt into lmms for 4d scene understanding. In: Proc. Int. Conf. Learn. Representations (2026) [4](#), [10](#), [12](#)
- [90] Zhou, J., Gao, H., Voleti, V., Vasishta, A., Yao, C.H., Boss, M., Torr, P., Rupprecht, C., Jampani, V.: Stable virtual camera: Generative view synthesis with diffusion models. In: Proc. IEEE Int. Conf. Comput. Vis. (2025) [5](#), [13](#), [25](#), [27](#), [28](#)
- [91] Zhu, C., Wang, T., Zhang, W., Pang, J., Liu, X.: Llava-3d: A simple yet effective pathway to empowering lmms with 3d-awareness. In: Proc. IEEE Int. Conf. Comput. Vis. (2024) [10](#)
- [92] Zhu, Z., Ma, X., Chen, Y., Deng, Z., Huang, S., Li, Q.: 3d-vista: Pre-trained transformer for 3d vision and text alignment. In: Proc. IEEE Int. Conf. Comput. Vis. (2023) [2](#), [10](#)

- [93] Zhu, Z., Zhang, Z., Ma, X., Niu, X., Chen, Y., Jia, B., Deng, Z., Huang, S., Li, Q.: Unifying 3d vision-language understanding via promptable queries. In: Proc. Eur. Conf. Comput. Vis. (2024) 10

# Supplementary Material

## A Technical Appendices

This supplementary material provides additional technical details of our method, including the overall training procedure, the detailed configurations of the compared visual backbones, the implementation details of the multi-view correspondence score, and the normalized overall score (NOS) analysis.

Algorithm 1 summarizes the training pipeline of VEGA-3D. It highlights how the semantic branch and the generative branch are constructed, aligned, and fused before the resulting visual tokens are passed to the language model.

---

### Algorithm 1 Training Pipeline with a Generative Visual Encoder and Feature Fusion

---

**Require:** Training set  $\mathcal{D} = \{(x_i, q_i, a_i)\}_{i=1}^N$ , sampled frame number  $K$ , semantic encoder  $E_{2D}$ , semantic projector  $P_{2D}$ , LLM  $M_\theta$ , generative source  $\sigma \in \{\text{offline}, \text{online}\}$

- 1: Initialize  $E_{2D}$ ,  $P_{2D}$ , and  $M_\theta$  from the stage-1 checkpoint
- 2: Build generative projector  $P_g$  and fusion module  $F$
- 3: **if**  $\sigma = \text{online}$  **then**
- 4:   Keep the generative encoder  $E_g$  frozen and instantiate it lazily at the first forward pass
- 5: **end if**
- 6: **for** each minibatch  $\mathcal{B} = \{(x_i, q_i, a_i)\}_{i=1}^B$  **do**
- 7:   **for** each sample  $(x_i, q_i, a_i)$  in  $\mathcal{B}$  **do**
- 8:      $\mathcal{V}_i \leftarrow \text{SAMPLEFRAMES}(x_i, K)$
- 9:      $\mathcal{W}_i \leftarrow \text{UNPROJECTDEPTHTOWORLD}(\mathcal{V}_i)$
- 10:      $\mathbf{Z}_i^{2d} \leftarrow P_{2D}(E_{2D}(\mathcal{V}_i))$
- 11:      $\mathbf{Z}_i^{2d} \leftarrow \text{POOLTO14X14}(\mathbf{Z}_i^{2d})$  ▷ 196 tokens per frame
- 12:     **if**  $\sigma = \text{offline}$  **then**
- 13:        $\mathbf{G}_i \leftarrow \text{LOADOFFLINEGENERATIVEFEATURES}(x_i)$
- 14:     **else**
- 15:        $\mathbf{G}_i \leftarrow \text{CACHEORENCODE}(E_g, \mathcal{V}_i)$  ▷ inference mode, no gradient
- 16:     **end if**
- 17:      $\mathbf{Z}_i^{gen} \leftarrow P_g(\text{FLATTENTOTOKENS}(\mathbf{G}_i))$
- 18:      $\mathbf{c}_i \leftarrow \text{BUILDINSTRUCTIONCONTEXT}(q_i)$  ▷ optional, for instruction-aware gating
- 19:      $\mathbf{Z}_i^{fuse} \leftarrow F(\mathbf{Z}_i^{2d}, \mathbf{Z}_i^{gen}, \mathbf{c}_i)$
- 20:      $\mathbf{Z}_i^{fuse} \leftarrow \mathbf{Z}_i^{fuse} + \text{3DPOSENC}(\mathcal{W}_i)$
- 21:      $\mathbf{X}_i^{vis} \leftarrow \text{SERIALIZEGRIDTOKENS}(\mathbf{Z}_i^{fuse})$
- 22:      $(\mathbf{e}_i, \mathbf{y}_i) \leftarrow \text{INSERTVISUALTOKENS}(q_i, a_i, \mathbf{X}_i^{vis})$  ▷ replace the special image token with visual tokens
- 23:   **end for**
- 24:    $\mathcal{L}_{LM} \leftarrow \frac{1}{B} \sum_{i=1}^B \text{CROSSENTROPY}(M_\theta(\mathbf{e}_i), \mathbf{y}_i)$
- 25:    $\mathcal{L} \leftarrow \mathcal{L}_{LM}$  ▷ optionally plus grounding loss
- 26:   Update the currently enabled trainable parameters  $\Theta$  using  $\nabla_{\Theta} \mathcal{L}$
- 27: **end for**

---

## B More Implementation Details

### B.1 Training Datasets

We summarize the training data used in our three experimental settings: 3D scene understanding, spatial reasoning, and robotic manipulation.

*3D scene understanding.* For the 3D scene understanding setting, we follow the same training-data protocol as Video-3D LLM [87]. Specifically, the model is trained in a multi-task manner on the combination of five public benchmarks: ScanRefer [9], Multi3DRefer [82], Scan2Cap [18], ScanQA [2], and SQA3D [53]. Following Video-3D LLM, these tasks are all built from ScanNet scenes [20] and are converted into video-style multi-view inputs for unified training. This setting covers the three main categories studied in our paper, i.e., 3D visual grounding, dense captioning, and question answering. We do not introduce additional 3D instruction-tuning corpora beyond this mixed training set, so that the comparison with the Video-3D LLM baseline remains controlled and fair.

*Spatial reasoning.* For spatial reasoning, we adopt the *S1* training set defined in VG-LLM [86]. In that work, *S1* denotes the default mixed training data composed of sampled instances from SPAR-7M and the LLaVA-Hound split of LLaVA-Video-178K. SPAR-7M provides spatially enriched supervision spanning diverse 3D reasoning skills, while the LLaVA-Hound split is included to preserve the general video-language capability of the backbone. Following the VG-LLM setting, we use only this *S1* mixture for training and do not incorporate the additional VLM-3R [22] data used in their extended ablation study. Therefore, our spatial reasoning results isolate the gain brought by generative priors under the same core data setting, without relying on extra task-specific synthetic supervision.

*Robotic manipulation.* For robotic manipulation, we directly use the standard LIBERO benchmark [48]. Following the protocol adopted by OpenVLA-OFT [40], we evaluate on the four canonical task suites: LIBERO-Spatial, LIBERO-Object, LIBERO-Goal, and LIBERO-Long. These suites are designed to test policy generalization under varying spatial layouts, object identities, goal conditions, and long-horizon task compositions, respectively. In our experiments, VEGA-3D is trained and evaluated on the same LIBERO downstream data as the OpenVLA-OFT baseline, without introducing additional robot datasets or auxiliary manipulation supervision, which keeps the comparison focused on the effect of our visual generative priors.

## B.2 Backbone Configurations for Tab. 4

Tab. A1 summarizes the detailed architecture and tokenization settings of the visual backbones compared in Tab. 4, including the discriminative models, the 3D foundation model, and the generative encoders. Unless otherwise noted, all extracted features are finally aligned to  $14 \times 14 = 196$  spatial tokens before fusion with the semantic branch.

**Tab-A1:** Detailed configurations of the visual backbones used in Tab. 4. “Native Tok.” denotes the token grid at the extracted feature stage before the final  $14 \times 14$  alignment. For token-based backbones such as ViTs and DiTs.

Model	Group	Architecture	Input Res.	Feature Stage	Patch Size	Native Tok.	Hidden Size
<i>Discriminative / self-supervised models</i>							
DINOv3-Large [62]	Self-supervised	ViT-L/16	$224 \times 224$	final patch tokens	16	196	1024
V-JEPA v2 [1]	Self-supervised	ViT-G/16	$224 \times 224$	encoder patch tokens	16	196	1408
<i>3D foundation model</i>							
VGGT [68]	Geometry	ViT-L/14 + aggregator	$196 \times 196$	last aggregator patch tokens	14	196	2048
<i>Generative models</i>							
Stable Video Diffusion [4]	Video diffusion	VAE + UNet	$896 \times 896$	UNet down block output	64	196	1280
Stable Diffusion 2.1 [61]	Image diffusion	VAE + UNet	$896 \times 896$	UNet pre-midblock feature	64	196	1280
Vmem [44]	Video diffusion	VAE + UNet	$896 \times 896$	final input-block feature	64	196	1280
SEVA [90]	Video diffusion	VAE + UNet	$896 \times 896$	final input-block feature	64	196	1280
VAE [61]	Autoencoder	VAE	$224 \times 224$	latent feature	16	196	4
Wan2.1-VACE [37]	Video diffusion	VAE + DiT	$1280 \times 720$	20th DiT block feature	16	3600	1536
Wan2.1-T2V [66]	Video diffusion	VAE + DiT	$1280 \times 720$	20th DiT block feature	16	3600	1536

## C Details of Multi-view Correspondence Score and Normalized Overall Score

### C.1 Multi-view Correspondence Score

The multi-view correspondence score used in Fig. 3 is not computed by exhaustively matching arbitrary token pairs from different frames. Instead, the implementation first associates each visual token with a 3D point and then only compares tokens that are assigned to the same voxel and come from different views.

Concretely, for each scene we uniformly sample up to 32 frames. Depth maps are unprojected into 3D world coordinates using the camera intrinsics and poses, and the poses are first transformed by the scene-specific axis-alignment matrix so that all views are expressed in a shared scene coordinate system. In the default analysis setting, the sampled images are resized to  $384 \times 384$  before feature extraction, and the dense world coordinates are resized with the same image transform. After extracting a feature map  $\mathbf{F} \in \mathbb{R}^{T \times C \times H_f \times W_f}$ , the world coordinates are temporally resampled if needed and then adaptively average-pooled to the same  $H_f \times W_f$  grid; in the default encoder setting, this corresponds to a  $14 \times 14$  token grid. Therefore, each feature token is paired with one pooled 3D point rather than with all raw pixels inside the corresponding image patch.

Let  $f_n \in \mathbb{R}^C$  denote the flattened token feature,  $x_n \in \mathbb{R}^3$  denote its pooled 3D coordinate, and  $v(n)$  denote its view index. The scene-specific voxel index is defined as

$$g(n) = \left\lfloor \frac{x_n - x_{\min}}{s} \right\rfloor, \quad (9)$$

where  $x_{\min}$  is the element-wise minimum of all token coordinates in the current scene and  $s$  is the voxel size, which is set to 0.1 m by default. For each voxel  $k$  and view  $t$ , we collect

$$\Omega_{k,t} = \{n \mid g(n) = k, v(n) = t\}. \quad (10)$$

If  $\Omega_{k,t}$  is non-empty, all tokens from the same view inside that voxel are first averaged and then L2-normalized to form a per-view prototype:

$$p_{k,t} = \text{Normalize} \left( \frac{1}{|\Omega_{k,t}|} \sum_{n \in \Omega_{k,t}} f_n \right). \quad (11)$$

Only voxels observed by at least two distinct views contribute to the final score. Denoting the set of such views for voxel  $k$  by  $V_k$ , the cross-view correspondence terms are

$$c_{k,t,t'} = p_{k,t}^\top p_{k,t'}, \quad t < t', \quad t, t' \in V_k. \quad (12)$$

The scene-level multi-view correspondence score is then computed as

$$S = \frac{\sum_k \sum_{t < t', t, t' \in V_k} c_{k,t,t'}}{\sum_k \binom{|V_k|}{2}}. \quad (13)$$

Several implementation details are important for reproducing the exact score. First, this is a *pair-weighted* average rather than a voxel-weighted average: a voxel observed by more views contributes more cross-view pairs. Second, tokens from the same view are never self-matched; multiple same-view tokens that fall into the same voxel are merged into one prototype before normalization. Third, the main correspondence script does not explicitly discard invalid depth pixels with zero depth, which differs from the visualization code path that applies an additional validity mask. Fourth, if a scene contains no voxel observed by at least two views, its score is recorded as NaN. Finally, dataset-level statistics are computed by first obtaining one score per scene and then reporting the mean and standard deviation over valid scene scores, rather than by globally aggregating all token pairs from all scenes into a single pool.

## C.2 Normalized Overall Score (NOS)

To summarize the overall downstream performance with a single scalar, we compute a Normalized Overall Score (NOS) by first normalizing each metric to  $[0, 1]$  and then averaging across all metrics. Importantly, the discriminative models and the generative models are normalized *separately*. In each group, we include the corresponding baseline when computing the per-metric minimum and maximum.

For a model  $t$  and metric  $m$ , the normalized score is defined as

$$\text{Norm}(x_{t,m}) = \frac{x_{t,m} - \min_{t' \in \mathcal{G}} x_{t',m}}{\max_{t' \in \mathcal{G}} x_{t',m} - \min_{t' \in \mathcal{G}} x_{t',m}}, \quad (14)$$

where  $\mathcal{G}$  denotes either the discriminative-model group or the generative-model group together with the baseline. We then compute

$$\text{NOS}(t) = \frac{100}{M} \sum_{m=1}^M \text{Norm}(x_{t,m}), \quad (15)$$

where the final factor of 100 converts the averaged normalized score into a percentage. Here  $M=9$  is the number of evaluation metrics used in Tab. 4, namely the ScanRefer accuracies at IoU thresholds 0.25 and 0.5 (Acc@0.25 and Acc@0.5), the Multi3DRefer F1 scores at IoU thresholds 0.25 and 0.5 (F1@0.25 and F1@0.5), the Scan2Cap captioning scores measured by CIDEr@0.5 and BLEU-4@0.5, the ScanQA question answering scores measured by CIDEr and exact match (EM), and the SQA3D exact match score.

Tab. A2 summarizes the final NOS values together with the multi-view correspondence scores used in the analysis. Since the raw task metrics are already reported in Tab. 4 of the main paper, we omit those dataset-wise results here.

**Tab-A2:** Summary of NOS and multi-view correspondence scores for the models in Tab. 4. Both NOS and correspondence scores are reported in percentage. NOS is computed separately for the discriminative group and the generative group, each together with the baseline; therefore, the baseline row reports two NOS values, in the order of discriminative / generative normalization. Bold denotes the best result in each group.

Models	NOS Score (%)	Correspondence Score (%)
Baseline	13.58 / 12.22	-
<i>Discriminative Models</i>		
V-JEPA v2 [1]	77.54	72.00
DINOv3-Large [62]	61.63	61.90
VGGT [68]	<b>88.24</b>	<b>77.21</b>
<i>Generative Models</i>		
Stable Video Diffusion [4]	52.06	17.95
Stable Diffusion 2.1 [61]	70.57	23.83
Vmem [44]	63.75	66.74
SEVA [90]	75.28	76.15
VAE [61]	77.29	79.69
Wan2.1-VACE [37]	<b>89.32</b>	<b>97.04</b>
Wan2.1-T2V [66]	82.41	96.88

## D Probe analysis of the 3D priors in Generation Models

Fig. 6 studies how the extracted generative prior changes with the diffusion timestep and the DiT depth. For completeness, we report the exact downstream results corresponding to Fig. 6 in Tabs. A3 and A5. We also provide additional timestep ablations for SEVA and Vmem in Tab. A4, which show a similar trend: intermediate timesteps generally yield stronger and more stable downstream performance than very late timesteps.

## E Additional Qualitative Results

We provide additional qualitative comparisons between VEGA-3D and the corresponding baseline models on ScanRefer and representative VSI-Bench sub-tasks. The success cases in Figs. 8, 10, 11, and 12 show that our method produces more

**Tab-A3:** Exact ablation results for different diffusion timesteps in Fig. 6(a). All rows use Wan2.1-T2V-1.3B, and only the sampling timestep is varied.

Timestep	ScanRefer		Multi3DRefer		Scan2Cap		ScanQA		SQA3D
	Acc. <sub>.25</sub>	Acc. <sub>.5</sub>	F1. <sub>.25</sub>	F1. <sub>.5</sub>	C. <sub>.5</sub>	B-4. <sub>.5</sub>	C	EM	EM
Baseline	58.1	51.7	58.0	52.7	83.8	41.3	102.1	30.1	58.6
0	62.4	55.6	60.6	55.0	82.3	42.0	106.3	30.2	60.9
100	61.3	54.3	60.0	54.4	81.7	41.8	106.1	30.0	61.5
200	61.9	55.0	60.1	54.7	83.1	42.4	107.6	30.6	60.7
300	63.2	56.2	60.8	55.1	83.2	42.2	106.3	30.4	61.3
400	62.4	55.3	60.3	54.6	84.3	42.6	105.1	29.9	60.7
500	61.8	55.2	59.8	54.4	81.7	42.1	106.6	31.1	61.4
600	62.1	55.1	60.2	54.6	83.2	42.2	105.0	30.1	61.1
700	62.2	55.4	60.5	55.0	80.6	41.7	105.6	30.3	61.2
800	62.1	55.3	60.0	54.6	82.7	41.7	106.4	30.5	60.7
900	61.6	54.7	59.7	54.3	81.4	41.9	107.7	30.8	61.0
1000	61.4	54.6	59.7	54.3	82.0	42.1	105.0	30.2	60.9

**Tab-A4:** Additional timestep ablations for SEVA [90] and Vmem [44]. Rows are grouped by backbone, and only the sampling timestep varies within each group. Similar to Wan2.1-T2V, both backbones tend to perform better at intermediate timesteps than at the end of the diffusion trajectory.

Timestep	ScanRefer		Multi3DRefer		Scan2Cap		ScanQA		SQA3D
	Acc. <sub>.25</sub>	Acc. <sub>.5</sub>	F1. <sub>.25</sub>	F1. <sub>.5</sub>	C. <sub>.5</sub>	B-4. <sub>.5</sub>	C	EM	EM
<i>SEVA</i>									
250	61.3	54.5	59.9	54.5	81.6	41.7	105.3	30.3	62.0
300	60.9	54.2	59.5	54.2	79.5	41.1	106.3	30.4	60.7
400	62.3	55.4	60.4	54.9	80.4	41.4	105.4	30.2	60.8
500	62.1	55.1	60.3	54.7	83.1	42.3	105.7	30.3	61.3
600	61.6	54.7	60.4	54.8	81.8	41.9	105.3	30.2	61.8
700	62.3	55.5	60.1	54.5	82.5	42.1	107.6	30.8	60.9
800	61.3	54.6	59.8	54.4	80.9	41.8	105.5	30.6	61.8
900	61.8	55.0	60.1	54.6	83.4	42.4	107.2	30.7	61.2
1000	61.4	54.3	59.6	54.1	81.6	42.0	105.7	30.7	61.1
<i>Vmem</i>									
250	62.5	55.7	60.5	54.9	80.9	41.5	105.8	30.3	61.7
300	62.5	55.7	60.2	54.7	82.0	41.9	106.0	29.9	61.4
400	62.0	55.0	60.4	54.9	81.1	41.7	105.6	30.3	60.7
500	62.1	55.2	60.2	54.6	81.8	41.6	104.8	30.0	60.8
600	62.3	55.5	60.5	55.0	81.4	41.7	105.5	30.4	61.4
700	62.0	55.0	60.2	54.6	81.3	41.8	105.3	30.1	61.4
800	61.2	54.3	59.3	53.7	80.6	41.4	107.3	30.7	60.7
900	61.9	54.9	60.1	54.6	81.3	42.1	107.1	30.3	61.5
1000	61.7	54.8	59.8	54.2	82.3	41.7	107.3	30.5	61.7

**Tab-A5:** Exact ablation results for different DiT blocks in Fig. 6(b). All rows use Wan2.1-T2V-1.3B at timestep  $k = 300$  under the  $1280 \times 720$  setting, and only the extracted DiT block is varied.

Block	ScanRefer		Multi3DRefer		Scan2Cap		ScanQA		SQA3D
	Acc. <sub>.25</sub>	Acc. <sub>.5</sub>	F1. <sub>.25</sub>	F1. <sub>.5</sub>	C. <sub>.5</sub>	B-4. <sub>.5</sub>	C	EM	EM
10	62.3	55.3	60.4	54.8	83.4	42.6	106.8	30.7	61.1
12	61.9	55.2	60.6	54.9	81.2	41.3	106.0	30.3	61.7
15	61.8	54.8	60.0	54.4	81.6	41.4	105.8	30.4	60.9
20	63.2	56.2	60.8	55.1	83.2	42.2	106.3	30.4	61.3
25	61.9	54.9	60.0	54.5	81.2	41.5	105.5	30.1	61.3
28	61.4	54.5	59.4	53.9	84.0	42.4	106.0	30.0	61.6

spatially grounded predictions: on ScanRefer, it localizes the target object more precisely in cluttered indoor scenes, and on VSI-Bench it handles appearance order, relative direction, and relative distance more reliably. We also include a representative ScanRefer failure case in Fig. 9. Even when VEGA-3D does not identify the exact target instance, its prediction remains close to the ground-truth region, suggesting that the generative prior substantially improves coarse spatial grounding while fine-grained disambiguation among nearby similar objects is still challenging.

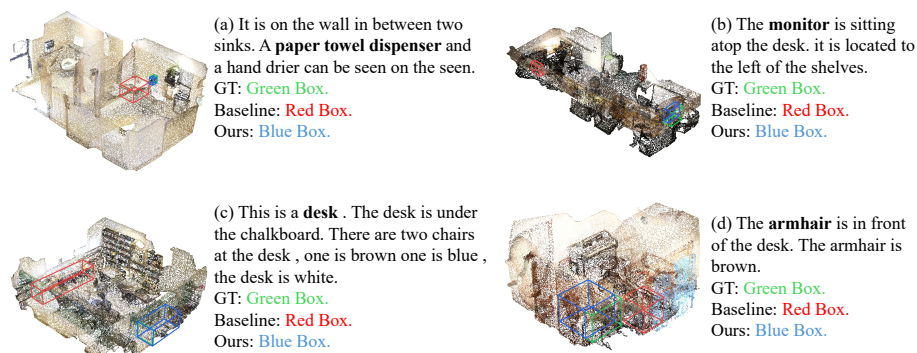


**Fig. 8:** Qualitative comparison on ScanRefer. Compared with the baseline, VEGA-3D localizes the referred object accurately under clutter, occlusion, and ambiguous referring expressions, reflecting stronger spatial grounding from the generative prior.

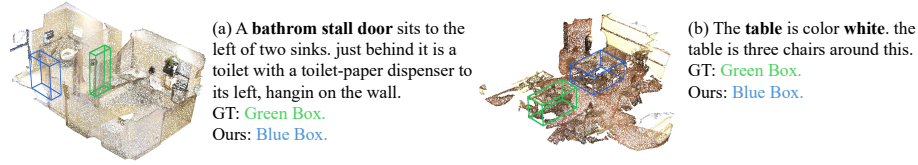


**Fig. 9:** Representative failure case on ScanRefer. We show the VEGA-3D prediction and the ground-truth box, indicating that VEGA-3D captures a reasonable spatial anchor but can still struggle with fine-grained instance disambiguation in cluttered scenes.

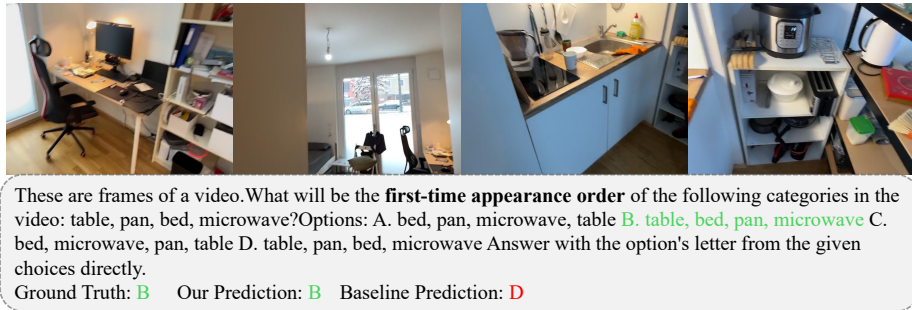


**Fig. 10:** Qualitative comparison on the Appearance Order subset of VSI-Bench. VEGA-3D better captures the ordering of object appearances and is less distracted by locally plausible but temporally inconsistent choices than the baseline.

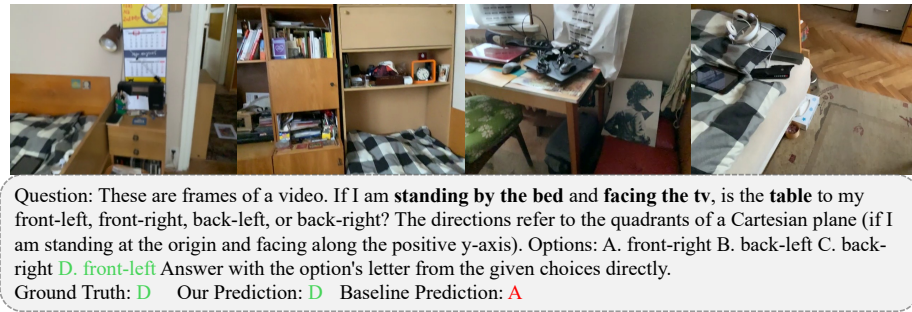


**Fig. 11:** Qualitative comparison on the Relative Direction subset of VSI-Bench. VEGA-3D yields reliable directional reasoning, such as left/right and front/behind relations, by grounding the decision in geometry-consistent visual features.

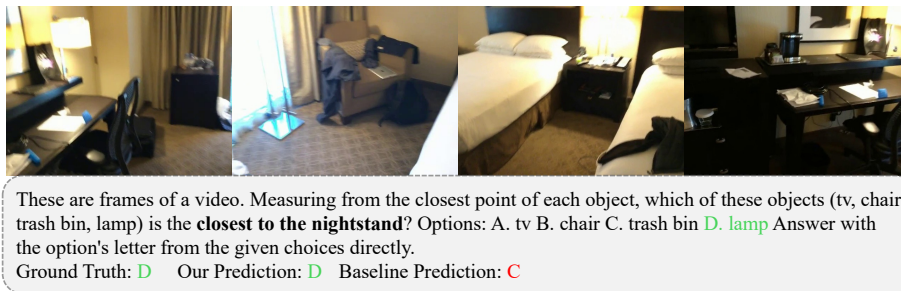


**Fig. 12:** Qualitative comparison on the Relative Distance subset of VSI-Bench. VEGA-3D distinguishes near/far relationships and relative depth ordering, whereas the baseline is prone to confuse objects with similar semantics but different spatial positions.

## F Limitations

At the same time, our study also highlights several limitations. First, generative priors are complementary to semantic features rather than a replacement for them: they help most on localization-centric and geometry-sensitive tasks, while semantic-heavy metrics such as captioning may improve less consistently. Second, not all generative backbones are equally suitable. In our analysis, DiT-based models exhibit substantially stronger multi-view consistency than several UNet-based alternatives, suggesting that transfer quality depends on the backbone architecture and pretraining regime. Third, incorporating a frozen video generator increases memory and inference cost, even though feature caching alleviates the overhead in practice. Finally, the best extraction setting currently depends on manually chosen intermediate timesteps and feature layers, and our experiments are still centered on indoor multi-view settings. Future work will study how to distill these priors into lighter encoders, learn more adaptive extraction strategies, and extend the framework to more dynamic and open-world environments.